The Pennsylvania State University

The Graduate School

College of Earth and Mineral Sciences

SEASONAL AND REGIONAL VARIABILITY IN TURBULENCE BELOW THE MIXED LAYER IN THE NORTH PACIFIC OCEAN

A Thesis in

Meteorology

by

Ryan P. Creedon

Submitted in Partial Fulfillment
of the Requirements
for the Degree of

Master of Science

May 2016

The thesis of Ryan P. Creedon was reviewed and approved* by the following:

Raymond G. Najjar
Professor of Meteorology
Thesis Adviser

Meghan F. Cronin
Oceanographer, Pacific Marine Environmental Laboratory

Marcelo Chamecki
Associate Adjunct Professor of Meteorology

Johannes Verlinde
Professor of Meteorology
Associate Head, Graduate Program in Meteorology

*Signatures are on file in the Graduate School.

ABSTRACT

Closures of upper-ocean heat budgets at National Oceanic and Atmospheric Administration North Pacific moorings KEO (32.3°N, 144.6°E) and Papa (50.1°N ,144.9°W) suggest seasonal and regional variability in turbulent diffusion below the mixed layer. Motivated by this variability, this investigation combines two years of hourly Acoustic Doppler Current Profiler velocities with subsurface density profiles at KEO and Papa to estimate hourly Richardson numbers (Ri) below the mixed layer. Prevalence of shear-based turbulence P_{SBT}, defined as the number of hours per day when Ri < 1 below the mixed layer, indicates potential occurrence of shear-based turbulence below the mixed layer from early to late spring at KEO and Papa. Moreover, P_{SBT} at KEO is found to be larger than at Papa throughout the investigation and may be attributed to enhanced velocity shears below mixed layer at KEO, particularly in spring. Such seasonal and regional variability in P_{SBT} resembles seasonal and regional variability found previously in diffusivities below the mixed layer. In particular, relatively large diffusivities during spring at KEO and Papa coincide with relatively large P_{SBT}, and large diffusivities at KEO year-round relative to those at Papa are reflected in higher P_{SBT} at KEO year-round. P_{SBT} is also found to be enhanced during early to late fall at KEO and Papa, distinct from seasonal variability in diffusivities. However, evidence of similar weekly variability between peaks in diffusivities and P_{SBT} is found at KEO during this time. In a separate analysis, diffusivities below the mixed layer are also found to correlate negatively with surface heat flux and positively with wind stress at KEO and Papa. These correlations are statistically significant at the 5% level and suggest local meteorological forcings on the ocean could present additional understanding of seasonal and regional variability observed in diffusivities below the mixed layer.

TABLE OF CONTENTS

LIST OF FIGURES

LIST OF TABLES

ACKNOWLEDGEMENTS

My sincerest thanks to the National Oceanic and Atmospheric Administration (NOAA) Ernest F. Hollings program for facilitating this collaboration between Penn State's Department of Meteorology and NOAA Pacific Marine Environmental Laboratory (PMEL). I also thank Nathan Anderson, research scientist and engineer at PMEL Ocean Climate Stations, for his assistance with Acoustic Doppler Current Profiler velocity data at NOAA moorings KEO and Papa. Lastly and most importantly, I thank my thesis co-advisers Raymond G. Najjar and Meghan F. Cronin for their support and guidance of this thesis.

Chapter 1

Introduction

The troposphere and upper-ocean are similar in vertical structure. A typical profile of potential temperature in the troposphere may be divided into three distinct layers: the well-mixed layer, the free troposphere, and the tropopause. Similarly, a typical profile of potential density in the upper-ocean may be divided into three distinct layers: the well-mixed layer, the pycnocline, and the abyssal (or deep) ocean. The ocean's well-mixed layer is directly in contact with the atmosphere and is characterized by uniform potential density to ~ 50 m mean depth, the pycnocline rests below the well-mixed layer and is characterized by potential density gradients due to sinking and equatorward movement of surface water at high latitudes, and the abyssal ocean rests below the pycnocline and is characterized by weak potential density gradients due to sinking of uniformly dense surface water from sub-polar regions. Thus, in both the troposphere and upper-ocean, two regions of weak static stability are separated by a strongly stable layer. Moreover, both possess well-mixed layers driven by convective and shear-based turbulence.

Turbulent diffusion, or mixing, occurs frequently between the ocean's well-mixed layer and seasonal pycnocline, a feature of the main pycnocline driven by diurnal and seasonal heating. This mixing instigates diffusive fluxes across the base of the mixed layer that can at times be first-order in upper-ocean heat and salinity budgets [*Cronin et al., 2013; Cronin et al., 2015*]. As a result, these fluxes are of fundamental importance for quantifying and parameterizing heat, momentum, and freshwater transport in the oceans [*Large et al., 1994; Canuto et al., 2001; Griffies et al., 2015*]. These fluxes also have significance to studies in

marine biogeochemistry. For instance, estimates of net community production in the North Pacific from upper-ocean carbon budgets [*Fassbender et al., 2016*] or initiation of phytoplankton blooms during springtime in the North Atlantic [*Mahadevan et al., 2012*] fundamentally rely on estimates of turbulent diffusion within and below the mixed layer.

Explanations for turbulent diffusion below the mixed layer have been proposed for several decades and vary extensively. One explanation suggests velocity shears associated with wind-generated, near-inertial oscillations (NIOs) propagate from the ocean surface to the interior, generating shear-based turbulence as they cross mixed layer base [*D'Asaro et al., 1985a*]. Recent observations illustrate that these NIOs are a result of variable winter winds in the subpolar Pacific [*Alfords et al., 2012*] and typhoons in the subtropical Pacific [*Bond et al., 2011*]. These studies found that when surface winds changed more rapidly than the inertial period, NIOs in ocean surface currents resulted. In addition, winds rotating anticyclonically at the inertial period were found to resonate with preexisting surface current NIOs.

An alternative explanation for turbulent diffusion below the mixed layer proposes that internal gravity waves excited in the deep ocean propagate through the seasonal pycnocline and break just below the mixed layer, initiating Kelvin-Helmholtz instabilities [*Woods, 1968; Garrett & Munk, 1979*]. A detailed investigation in the subtropical Atlantic observes the ability of these internal gravity waves to generate significant mixing from billows of Kelvin-Helmholtz instabilities [*van Haren & Gostiaux, 2012*]. These instabilities may also occur as a result of convective overturning cells generated by surface buoyancy loss, which provides yet another explanation for the presence of turbulent diffusion below the mixed layer [*Large et al., 1986; Large et al., 1994*].

Turbulent diffusion resulting from shear-based turbulence below the mixed layer is typically characterized by local velocity shear and density stratification. In particular, the effect of shear and stratification on stability below the mixed layer may be quantified using the gradient Richardson number (Ri):

$$[Eqn.\,1] \qquad Ri = \frac{\frac{-g}{\rho_0}\frac{\partial \sigma_\theta}{\partial z}}{(\frac{\partial u}{\partial z})^2 + (\frac{\partial v}{\partial z})^2} = \frac{N^2}{|\frac{\partial \boldsymbol{u}}{\partial z}|^2}$$

where g is the gravitational acceleration constant (9.81 m s^{-2}) , ρ_0 is a reference density (1027 kg m^{-3} for seawater), σ_θ is potential density minus 1000 kg m^{-3}, z is the vertical coordinate (positive upward), and u and v are the zonal and meridional velocity components, respectively. For conciseness, the numerator in [*Eqn. 1*] is often expressed as N^2 where N is the Brunt-Väisälä or buoyancy frequency. Likewise, the denominator is expressed in terms of the squared magnitude of velocity shear where $\boldsymbol{u}$ is the horizontal velocity vector.

Experimental and theoretical work suggest onset of shear-based turbulence in an initially laminar flow occurs when Richardson numbers are smaller than ~ ¼ and remain turbulent until Richardson numbers rise above ~ 1 [*Miles, 1961; Howard, 1961; Abarbanel et al., 1984; Stull, 1988; Nihoul & Jamart, 1988*]. Such definitive hysteresis, however, is not frequently achieved in geophysical applications, and so values for which Richardson numbers suggest turbulent flow may range from 0 to 1 [*Galperin et al., 2007*]. *Abarbanel et al. (1984)* and *Canuto et al. (2001)* suggest Ri $\leq$ 1 is a sufficient criteria for onset of shear-based turbulence based on laboratory measurements, nonlinear stability analysis, and large eddy simulation—with the implication

Richardson numbers exceeding unity indicate little chance, if any, for shear-based turbulence to occur.

Scalar fluxes $F_{turb,-h}$ associated with general turbulent diffusion below the mixed layer may be estimated to first-order using K-theory, which assumes $F_{turb,-h}$ is proportional to the vertical downgradient of a scalar ξ below mixed layer base [*Stull, 1988; Nihoul & Jamart, 1988*]:

$$[Eqn.\,2] \qquad F_{turb,-h} = -\kappa_\xi \frac{\partial \xi}{\partial z}|_{-h}$$

where κ_ξ is referred to as the diffusion coefficient or eddy diffusivity for scalar ξ, and h is the mixed layer depth. In this analysis, ξ will be given by temperature T, and the diffusion coefficient for temperature T will be hereinafter abbreviated to diffusivity. Dimensional arguments first demonstrated by Ludwig Prandtl show diffusivity is proportional to the product of a mixing length scale and square root of turbulent kinetic energy, from which diffusivity gains interpretation as the efficiency of turbulent mixing [*Nihoul & Jamart, 1988; Holton & Hakim, 2012*].

Diffusivities associated with turbulent diffusive fluxes below the mixed layer have been recently investigated at National Oceanic and Atmospheric Administration (NOAA) moorings KEO, or Kuroshio Extension Observatory, (32.3°N, 144.6°E) and Papa (50.1°N, 144.9°W) [*Cronin et al., 2013; Cronin et al., 2015*] [**Figure 1**]. These diffusivities were found by closing the *Stevenson and Niller (1983)* upper-ocean heat budget at both moorings:

$$[Eqn.\,3] \qquad \rho_0 c_p h \frac{\partial T_a}{\partial t}$$

$$= Q_0 - Q_{pen,-h} - \rho_0 c_p h \boldsymbol{u_a} \cdot \boldsymbol{\nabla} T_a - \rho_0 c_p \left(w_{-h} + \frac{dh}{dt} \right) (T_a - T_{-h}) - F_{turb,-h}$$

where ρ_0 and c_p are taken as a reference seawater density and specific heat capacity, respectively; h is mixed layer depth; Q_0 is net surface heat flux (positive into ocean); $Q_{pen,-h}$ is the net radiation penetrating out the base of the mixed layer (positive out mixed layer base); T_a and $\boldsymbol{u_a}$ are vertically averaged mixed layer temperature and horizontal velocity, respectively; T_{-h} and w_{-h} are temperature and vertical velocity immediately below mixed layer base, respectively; and $F_{turb,-h}$ is as described in [*Eqn. 2*] with ξ as T.

Buoy, float, and satellite measurements were used to estimate the first five terms of [*Eqn. 3*]. The residual of the balance after error analysis was $F_{turb,-h}$, and, using [*Eqn. 2*] with T as ξ, diffusivities below the mixed layer were estimated at KEO and Papa. Results suggest significant seasonal and regional variability in monthly and 5-day averaged diffusivities [*Cronin et al., 2015*]. In particular, diffusivities at both moorings achieve their greatest values during late winter and early spring, and diffusivities at KEO tend to be larger than those at Papa year-round. Such variability is, at present, becoming better represented in global ocean circulation models, but history indicates diffusivities immediately below mixed layer base were often assumed constant or as adjustable parameters not long ago [*Canuto et al., 2001*] and continue to be a challenge today.

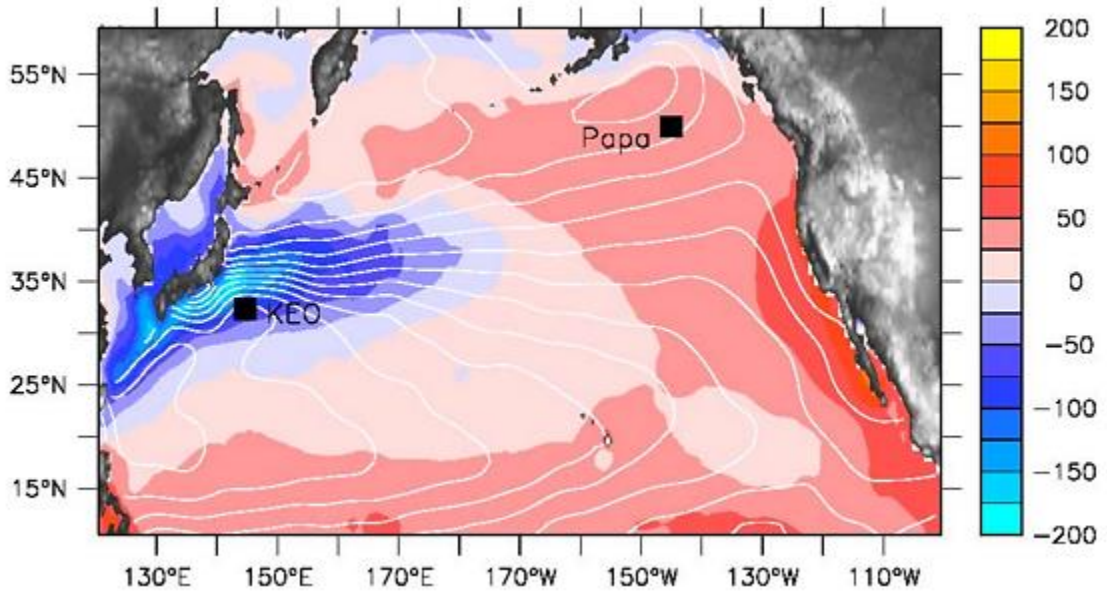

Figure 1. Location of Ocean Climate Stations KEO and Papa (black squares) with climatological net surface heat flux (in W m^{-2}) and surface height contours (grey lines) overlaid. Positive heat fluxes indicate ocean heat gain from atmosphere. Reproduced from *Cronin et al. (2015)*.

This thesis considers factors which may associate with seasonal and regional variability of diffusivities below the mixed layer in the North Pacific Ocean. By combining two years of hourly Acoustic Doppler Current Profiler (ADCP) velocities and subsurface density profiles at KEO and Papa, hourly Richardson number time series are computed at both moorings using [*Eqn. 1*]. Density stratification and velocity shears are then considered when Ri > 1 and Ri < 1 to compare conditions under which Richardson numbers suggest shear-based turbulence at KEO and Papa. Peaks in prevalence of shear-based turbulence, defined as the number of hours per day when Ri < 1, are then compared with peaks in diffusivities to determine associations between the prevalence of shear-based turbulence below the mixed layer and enhanced values of diffusivity. Diffusivities are also correlated with surface heat flux and wind stress to understand associations between local meteorological conditions and turbulent diffusion below the mixed layer.

While seminal works of *D'Asaro (1985b)*, *Large et al. (1986)*, *Shay (1992)*, and *Large & Crawford (1996)* have addressed upper-ocean Richardson number response to short-term and isolated surface forcing events in the mid-latitudes and tropics, this investigation considers prolonged time series of hourly bulk Richardson numbers below the mixed layer and compares them between seasons and between subtropical and subpolar ocean moorings for the first time. Moreover, while several parameterizations for diffusivity have been inspired by laboratory experiments or observations from the above works [*Gargett & Munk, 1979; Large et al., 1994; Canuto et al., 2001*], this investigation directly correlates 5-day diffusivities below the mixed layer with surface forcings and considers the seasonality of these associations. In so doing, this thesis seeks to provide physical connections to the variability in strength of turbulent diffusion critical to physical, chemical, and biological descriptions of the upper-ocean.

Chapter 2

Data

Data at Ocean Climate Station KEO

KEO began operation in June 2004 as part of the Kuroshio Extension System Study (KESS). During and after KESS, KEO was run by the Ocean Climate Station (OCS) group at NOAA's Pacific Marine Environmental Laboratory (PMEL) in Seattle, Washington. Since beginning its operation, KEO has been equipped with an ensemble of meteorological and subsurface sensors, including radiative instruments (pyranometer for downwelling shortwave/pyregeometer for downwelling longwave), sonic anemometers, subsurface temperature thermistors, and subsurface salinity conductivity cells. The sampling rate of radiation measurements is once per 2 minutes during this investigation and is accurate to within 1%. The sonic anemometers sample at the same rate and are accurate to within 2%. The subsurface thermistors and conductivity cells sample once per 10 minutes at 26 depths from 1 m to 525 m. The accuracy of the temperature and salinity measurements is ± 0.02°C and ~ ± 0.02 psu, repsectively [*Freitag et al., 1999*].

During KESS, an upward-looking ADCP was deployed on a nearby mooring with nominal coordinates (32.2°N, 144.3°E). The ADCP measured horizontal velocities at 150 kHz in 10 m intervals from ~ 50 m to ~ 250 m depth and will be used to estimate velocity shear profiles at KEO.

Data at Ocean Climate Station Papa

In contrast to KEO, Papa has been in operation in the northeastern subtropical Pacific Ocean under OCS since June 2007. Papa is equipped with a similar ensemble of instruments as KEO, including radiative instruments, sonic anemometers, subsurface temperature thermistors, and subsurface salinity conductivity cells. Sampling rates and accuracies of all measurements are the same as at KEO. However, subsurface thermistors and conductivity cells are located at 18 depths from 1 m to 200 m.

During 2007 to 2010, upward-looking ADCPs were deployed on a nearby mooring with nominal coordinates (50.1°N, 150.0°W). In 2007, the ADCP sampled horizontal velocities at 150 kHz in 4 m bins from 8 m to 128 m. During 2008, an upward looking 75 kHz ADCP at 800 m depth was paired with a 300 kHz ADCP at 154 m depth as part of a study by *Alfords et al. (2012)*. In addition, during 2009 to 2010, this study also placed an upward looking 75 hKz ADCP at 800 m depth and paired this ADCP with a 150 kHz ADCP at 227 m depth. Velocities were recorded in 2 m bins from 16 m to 208 m (and coarser resolution below 208 m to 800 m depth). Just as at KEO, these ADCP measurements are used to estimate velocity shear at Papa in this investigation.

During the 2008 and 2009 summers at Papa (June, July, and August), mixed layer depth frequently shoaled above the shallowest ADCP measurements. Therefore, in addition to ADCP velocity profiles, subsurface current meters positioned at 5 m, 15 m, and 35 m depth are used to supplement horizontal velocity profiles at Papa. These current meter measurements have accuracies up to 0.5 cm s^{-1} (within ~ 5% of typical recorded velocities).

Surface Forcings at KEO and Papa

From radiative and subsurface temperature measurements, net shortwave (SW_{net}) and longwave radiation (LW_{net}) may be estimated every 10 minutes at the air-sea interface for both KEO and Papa. In particular, SW_{net} may be estimated by modulating downwelling shortwave radiation measurements with sea surface albedo, assumed to be 0.055. LW_{net} may be estimated by subtracting downwelling longwave radiation measurements from estimated upwelling longwave radiation (derived from Stefan-Boltzmann law using shallowest subsurface temperature measurement) and then modulating the difference by a broadband sea surface emissivity, assumed to be 0.97. Latent and sensible heat fluxes at the air-sea interface (Q_{lat} and Q_{sen}, respectively) require greater sophistication to estimate every 10 mintutes; the algorithm involved is detailed in *Fairall, et al. (2003)*. Once these estimates are determined, net surface heat flux Q_0 may be estimated according to [*Eqn. 4*].

$$[Eqn.\,4] \qquad Q_0 = SW_{net} - LW_{net} - Q_{lat} - Q_{sen}$$

Positive values of Q_0 indicate net heat uptake by the ocean; negative values of Q_0 indicate net heat uptake by the atmosphere. Time series of Q_0 are block averaged to daily mean time series at both KEO and Papa and may be accessed at the following OCS webpage: http://www.pmel.noaa.gov/ocs/data/fluxdisdel/.

Zonal and meridional wind stress at the air-sea interface may also be estimated at KEO and Papa from measurements of 10 minute zonal and meridional winds using bulk scaling theory with stability-dependent transfer coefficients. Zonal and meridional wind stress may then be

combined in the usual sense to yield wind stress magnitude after accounting for "gustiness," or subgrid wind variability, as described in *Fairall et al. (2003)*. Time series of 10 minute wind stress magnitude are then block averaged to daily mean time series at KEO and Papa and may be accessed at the same OCS webpage as daily mean net surface heat flux time series.

Data Overview

All temperature, salinity, and ADCP data are recorded hourly (or averaged hourly) at KEO and Papa. Supplementary current meters at Papa are likewise recorded hourly. Temperature and salinity profiles are combined to yield hourly potential density profiles based on the international equation of state for seawater [*Millero & Poisson, 1981*]. These potential density profiles are calculated during June 2004 to November 2005 at KEO, when ADCP data are available and temperature and salinity measurements are free of major data gaps. Density profiles at Papa are calculated during June 2007 to June 2010 also to match ADCP data availability. However, density profiles from June 2008 to June 2009 are omitted as the Papa mooring broke from its anchor and, thus, only telemetered daily average profiles are available.

Data used to draw correlations between diffusivity and surface forcings include 5-day smoothed daily diffusivities, daily surface heat fluxes, and daily wind stresses during 2004 to 2014 at KEO and 2007 to 2013 at Papa. 5-day smoothed daily diffusivities, as well as corresponding 68% uncertainty estimates, are provided from the work of *Cronin et al. (2015)* described in the introduction and are the highest resolution available. Daily surface heat fluxes and wind stresses are provided by OCS, as described in the previous sub-section. These daily

time series are then 5-day smoothed with a 5-day triangular filter to match treatment of diffusivity time series.

Chapter 3

Methods

Richardson Numbers

Hourly density profiles at KEO and Papa frequently suffered from missing data between depth levels. Thus, small gaps in density profile data (≤ 20 m) were filled linearly at each mooring. It is assumed 20 m was sufficiently small so that density varied approximately linearly between two depths.

Hourly mixed layer depth at KEO and Papa was then calculated as a density step of 0.03 kg m^{-3} from hourly density at 10 m to match methods of diffusivity estimations below the mixed layer in *Cronin et al. (2015)*. Typical errors associated with this choice of estimation are on the order of 5 m [*Cronin et al., 2015; deBoyer Montégut, 2004*]. For convenience, density was then interpolated onto the same 1 m grid as ADCP velocity data. Hourly density stratification below the mixed layer was then estimated as a finite difference between density at the mixed layer depth and density 20 m below the mixed layer depth. Both components of hourly velocity gradients were estimated in a similar manner below the mixed layer at KEO and Papa using ADCP data, except during summer at Papa, when current meter data were used. From hourly density and velocity gradients below the mixed layer, hourly Richardson number time series below the mixed layer at KEO and Papa were estimated using [*Eqn. 1*]. Propagating errors in

density and velocity profiles detailed in the previous sub-section to Richardson number calculations suggests Richardson numbers are accurate to within ~ 7% of estimated values.

Stratification and Shear Comparisons

Given hourly Richardson number estimates at KEO and Papa, the number of hours each day when Richardson numbers fell below 1 and ¼ were counted. These critical Richardson numbers were selected as indicating potential for shear-based turbulent conditions [*Galperin et al., 2007*]. To allow for adequate comparisons between KEO and Papa and follow recommendations from *Abarbanel et al. (1984)* and *Canuto et al. (2001),* the choice of critical Richardson number was relaxed to 1. As a result, the number of hours per day for which Ri < 1 is hereinafter analyzed exclusively and is referred to as prevalence of shear-based turbulence (P_{SBT}) at KEO and Papa.

During March to April at KEO and April to June at Papa (when P_{SBT} was particularly high), distributions of density stratification and velocity shear were computed for Ri < 1 and Ri > 1. Differences in medians between corresponding density and velocity distributions at KEO and Papa were tested for statistical significance using Mood's statistic, offering a non-dimensional representation for the distance between medians of two samples [*Brown & Mood, 1951*]. Mood's statistic was chosen over the familiar Student's two sample T-test for difference of means due to non-normal density stratification and velocity shear distributions. Given the level of significance chosen for this analysis is 5%, any Mood's statistic in excess of 3.84 suggested statistically different medians [*Brown & Mood, 1951*].

Richardson Number and Diffusivity Associations

P_{SBT} was smoothed using a 5–day triangular running average to mimic treatment of diffusivities in *Cronin et al. [2015]*. Local peaks of P_{SBT}, defined as days for which P_{SBT} were larger than immediately previous and following days, were identified at KEO and Papa. Local peaks of diffusivities were obtained similarly. The mean number of days between local peaks of P_{SBT} and diffusivities was calculated at KEO during summer and fall and interpreted as mean peak periodicity T. The mean number of days between local peaks of P_{SBT} and diffusivities was not calculated at Papa or during winter and spring seasons at KEO due to weak P_{SBT} signals and heavily discontinuous data. Standard errors (SE) were calculated for T according to [*Eqn. 5*]:

$$[Eqn. 5] \qquad SE = \frac{s_p}{\sqrt{n_p}}$$

where s_p is the sample standard deviation of the number of days between peaks and n_p is the number of peaks observed. From these estimates of standard errors, the mean periodicity of peaks in turbulence prevalence and diffusivities were compared using a two-sample, two-sided Student T-test with significance level at 5%. Student's two-sided T-test is used in this section, as opposed to the previous, since distributions of T are found to be approximately normal.

In addition, the mean distance between peaks of P_{SBT} and diffusivities (d_f) were calculated at KEO during summer and fall seasons, where distance between peaks was defined as the shortest number of days between a peak in turbulence prevalence and a peak in diffusivity.

These distances were not recorded at Papa or during winter and spring at KEO also as a result of weak P_{SBT} signals and heavily discontinuous data.

In order to insure mean periodicity of peaks in P_{SBT} and diffusivities was not a side-effect of the 5-day smoothing on both time series, a traditional spectral analysis as described in *Bendat & Piersol (2011)* was performed on P_{SBT} before and after smoothing to understand the quantitative effect of smoothing on modes of variability in P_{SBT}. If spectra corresponding to frequencies from the peak analysis were preserved post-smoothing and found to be of similar order of magnitude (no different than ~ 5-fold difference), then it was assumed periodicity of peaks in P_{SBT} was not entirely a result of smoothing, but also of natural variability.

This spectral analysis was limited to late summer and early fall at KEO, as P_{SBT} was near-continuous during this time period (a requirement of spectral analysis) and its signal was sufficiently robust to warrant spectral analysis (whereas at Papa, $P_{SBT} \sim 0$ throughout this time period, as will be seen). Though this spectral analysis cannot be performed on diffusivities due to lack of a true daily time series, it is assumed the 5-day smoother will have had similar effect on diffusivities.

Surface Forcing and Diffusivity Associations

5-day smoothed diffusivity, surface heat flux, and wind stress time series were considered only when all three variables were available at each mooring. Resulting time series were subsampled every three days to filter out effects of the 5-day smoothing, which was found to introduce significant autoregression in all variables out to the second time lag at both moorings.

This filtering process was done so that each time series exhibited minimal autocorrelation, which would otherwise violate assumptions of linear correlation analysis [*Montgomery & Runger, 2011*].

Subsampled diffusivities, surface heat fluxes, and wind stresses were binned and concatenated into the following six bi-months at KEO and Papa: January to February, March to April, May to June, July to August, September to October, and November to December. The choice of bi-months stemmed from the desire to understand seasonal variability of associations between diffusivity and surface forcings and insufficient sample sizes for correlation analysis if monthly binning of data was chosen instead.

In each bi-month, time series *x* were standardized as follows:

$$[Eqn.\,6] \qquad z_x = \frac{x - x_{avg}}{s_x}$$

where z_x is the standardized time series corresponding to *x*, x_{avg} is the mean of *x* over a bi-month, and s_x is the standard deviation of *x* over a bi-month. Time series were standardized so as to non-dimensionalize forthcoming regression coefficients.

Underlying assumptions of simple linear regression were checked before correlating standardized, subsampled time series of diffusivities with those of heat flux and wind stress for each bi-month at KEO and Papa. These assumptions included the following:

1. Minimal autocorrelation within all time series.
2. No multi-collinearity, or significant correlation, between heat flux and wind stress time series.

3. Homoscedasticity, or equal variance among well-representative samples of all time series.
4. Minimal autocorrelation within residuals of regression (i.e., no serial correlation).
5. Linear relationship between diffusivities, heat fluxes, and wind stresses.

Assumption 1 was treated by subsampling time series. Assumptions 2-4 were treated by variance inflation factors (VIF), the Breusch-Pagan test, and the Durbin-Watson statistic, respectively. Explanations for these statistical methods may be found in *Montgomery & Runger (2011)*, *Breusch & Pagan (1979)*, and *McAuliffe (2005)*, respectively. Assumption 5 was assumed a priori for lack of a true physical relationship. Violations in any of the assumptions result in underestimation of standard errors of regression coefficients and, thus, overestimation of confidence in the robustness of these coefficients.

For all bi-months, time series of surface heat flux and wind stress exhibited multi-collinearity according to VIFs, violating the second assumption. This violation was anticipated, as heat flux and wind stress often vary with local meteorological conditions. To avoid multi-collinearity, diffusivities were regressed against heat flux and wind stress separately. Hence, for each bi-month at both KEO and Papa, correlation analysis was linear and simple, with only one independent variable considered at a time. If assumptions 3 or 4 were violated for any given bi-month, the simple linear correlation was rectified using the method of *Andrews (1991)* to obtain new, unbiased estimates of standard errors for regression coefficients. Radii of 95% confidence intervals for regression coefficients were then obtained by multiplying standard errors by 1.96.

In total, 24 simple linear regressions were performed: 12 at KEO and 12 at Papa. The 12 regressions at KEO consisted of two regressions for each bi-month: one regression between

diffusivity and surface heat flux and one regression between diffusivity and wind stress. The 12 regressions at Papa were divided similarly. Corresponding regression coefficients between KEO and Papa were directly compared via Student's T-test according to *Paternoster et al. (1998)* and interpreted as the relative strength of sensitivity between diffusivities and surface forcings [*Johnson & LeBreton, 2004*]. Distributions of regression coefficients were assumed normal so that Student's T-test may be used to compare regression coefficients. The equation for the appropriate Student's T-test statistic (*t*) according to *Paternoster et al. (1998)* is the following:

$$[Eqn.7] \qquad t = \frac{\beta_2 - \beta_1}{\sqrt{SE_1^2 + SE_2^2}}$$

where β_1 is a regression coefficient at KEO, β_2 is the corresponding regression coefficient at Papa, SE_1 is the standard error of the regression coefficient at KEO, and SE_2 is the standard error of the corresponding regression coefficient at Papa.

Chapter 5

Results

Richardson Numbers

According to **Figure 2**, average mixed layer density varies considerably at KEO, from σ_θ ~ 21. 5 kg m^{-3} in summer to ~ 25.5 kg m^{-3} in winter. Such seasonality is also reflected in mixed layer depth, which shoals close to the ocean surface in summer and dives well below 150 m in winter. By comparison, average mixed layer density at Papa displays significantly less seasonality, and Papa's mixed layer depth, though similar to KEO's during summer, is far shallower in winter by several tens of meters.

Seasonality of average mixed layer density is responsible for seasonality observed in buoyancy frequency below mixed layer base at KEO and Papa. As **Figure 3** shows, squared buoyancy frequency at KEO varies from ~ 4×10^{-4} s^{-2} during summer, when the ocean is well-stratified below mixed layer, to ~ 1×10^{-5} s^{-2} during late winter, when the upper-ocean is nearly homogeneous. Buoyancy frequency at Papa displays similar seasonality; however, extreme values of ~ 4×10^{-4} s^{-2} and ~ 1×10^{-5} s^{-2} are not as sustained as at KEO, as the lifespan of Papa's seasonal pycnocline is shorter than that at KEO according to **Figure 4** and longer density profile records provided by OCS.

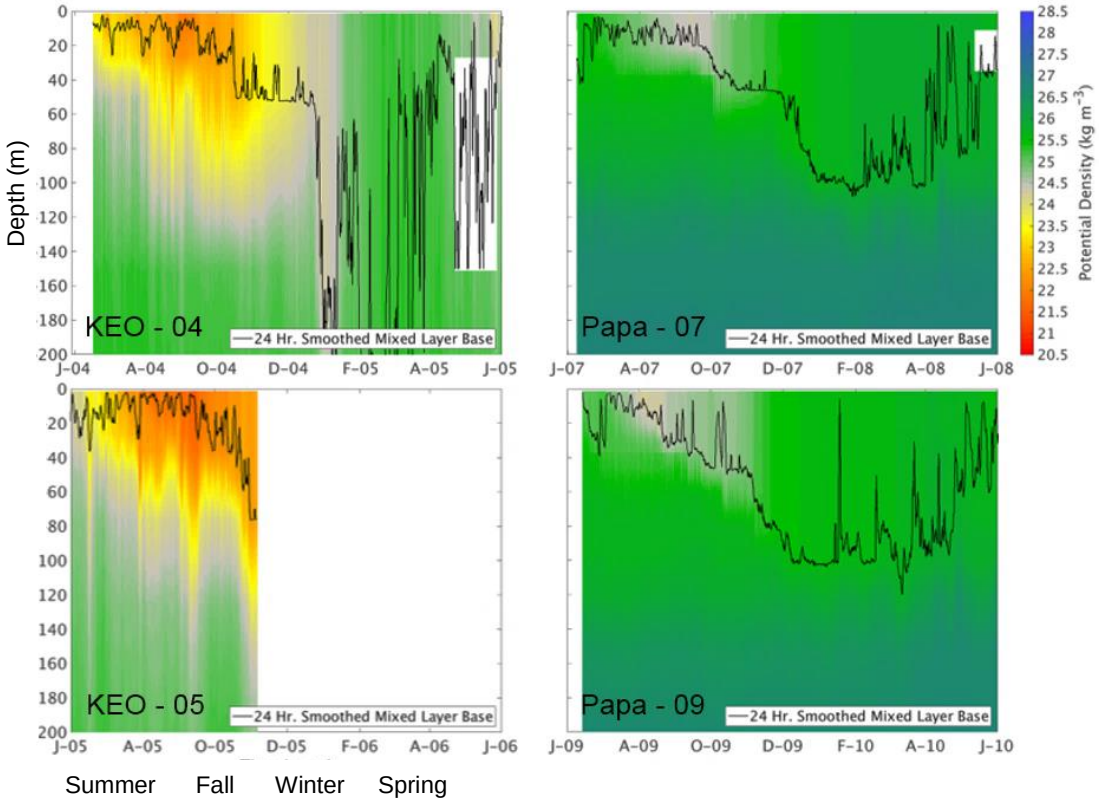

Figure 2. Left panels: hourly potential density profiles at KEO for June 2004 to 2005 (top) and for June 2005 to 2006 (bottom). Right panels: hourly potential density profiles at Papa for June 2007 to 2008 (top) and for June 2009 to 2010 (bottom). White space indicates gaps in potential density profiles > 20 m thickness. Corresponding 24 hour smoothed mixed layer depth derived from hourly potential density profiles is overlaid in black.

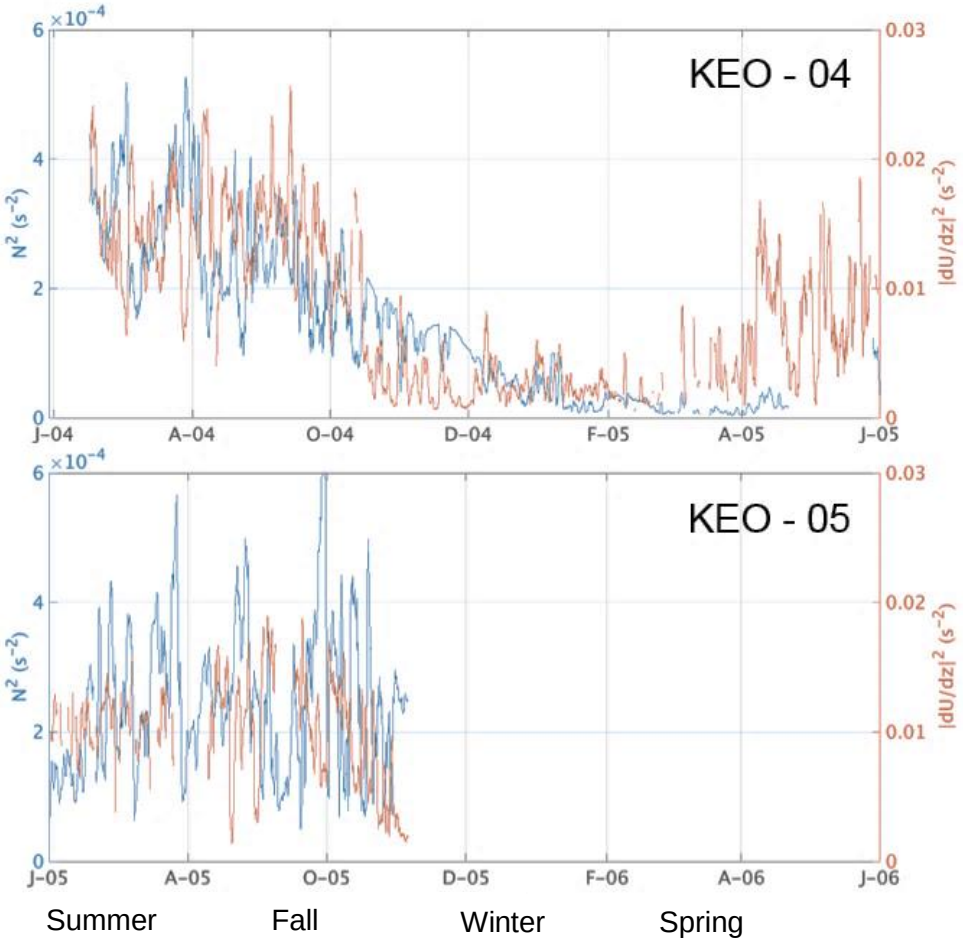

Figure 3. Hourly squared buoyancy frequency (blue) and squared velocity shear (orange) below the mixed layer at KEO for June 2004 to 2005 (top) and for June 2005 to 2006 (bottom).

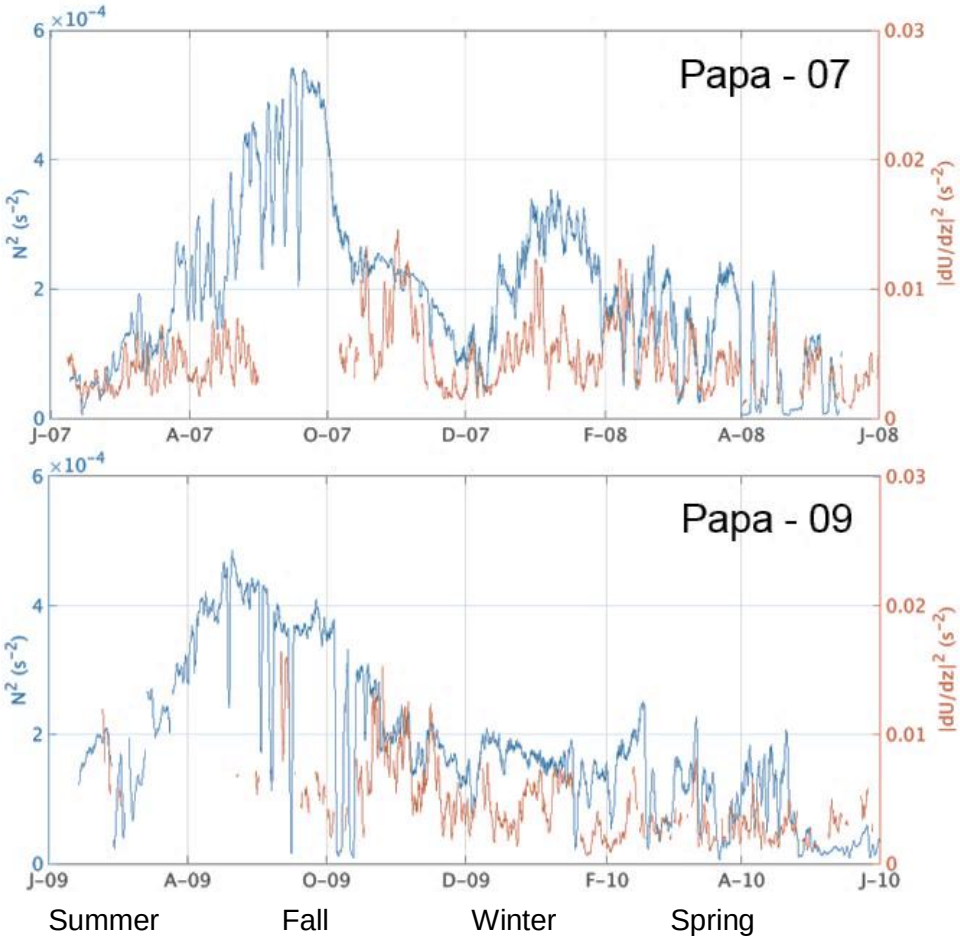

Figure 4. Hourly squared buoyancy frequency (blue) and squared velocity shear (orange) below the mixed layer at Papa for June 2007 to 2008 (top) and for June 2009 to 2010 (bottom).

Differences in squared buoyancy frequency and velocity shear between KEO and Papa are more apparent in **Table 1**, which provides estimates of mean surface heat flux, wind stress, mixed layer depth, stratification, and velocity shear from October to March and April to September at KEO and Papa.

Table 1. Average values of surface heat flux, surface wind stress, mixed layer depth, squared buoyancy frequency below mixed layer, and squared velocity shear below mixed layer at KEO and Papa during October-March and April-September.

Variable	**KEO**		**Papa**	
	Oct.-Mar.	Apr.-Sept.	Oct.-Mar.	Apr.-Sept.
Surface Heat Flux (W m^{-2})	-190	110	-60	120
Surface Wind Stress (N m^{-2})	0.18	0.09	0.24	0.11
Mixed Layer Depth (m)	117	55	84	39
N^2 (s^{-2})	0.96×10^{-4}	2.2×10^{-4}	1.7×10^{-4}	1.9×10^{-4}
$\left\lvert \frac{\partial u}{\partial z} \right\rvert^2$ ***(s^{-2})***	1.7×10^{-5}	140×10^{-5}	2.5×10^{-5}	1.8×10^{-5}

According to **Table 1**, KEO experiences larger seasonality in both density stratification and velocity shear, and thus N^2 and $\left\lvert \frac{\partial u}{\partial z} \right\rvert^2$, below the mixed layer than at Papa. Moreover, annual average density stratification is stronger at Papa, while annual average velocity shear is stronger at KEO (though this could be an anomaly given velocity shear data is provided for only ~ 1.4 years).

Stronger stratification at Papa may attributed to less surface ocean heat loss during winter, as seen in **Table 1**. Indeed, the juxtaposition of the nearby Kuroshio warm current and cold, continental air masses will moderate mixed layer density at KEO significantly compared to Papa's maritime location, allowing for significantly weaker density stratification below the mixed layer during early spring at KEO [*Qiu & Kelly, 1993*]. Stronger stratification at Papa may also be attributed to a stronger halocline at Papa, as noted in *Cronin et al. (2015)*, or to stronger upwelling due to the presence of a cyclonic, subpolar gyre at Papa.

Stronger annual mean velocity shears at KEO appear to result from stronger subsurface velocities in the mixed layer relative to velocities well-below the mixed layer throughout the year, especially during summer. Indeed, horizontal velocity magnitudes average ~ 0.40 m s^{-1} year-round at KEO down to 50 m depth and begin decay below 50 m. Velocity profiles at KEO (not pictured) also exhibit extended periods of time (on the order of months) when the sign of horizontal velocity components remain unchanged across all observed depths, which may be due to the larger-scaled current system associated with the meandering Kuroshio Extension and detached rings [*Mizuno & White, 1983; Qiu & Chen, 2005*]. In contrast, at Papa, mean horizontal velocity magnitudes are on the order of ~ 0.10 m s^{-1} year-round down to 50 m depth, smaller than at KEO. Larger magnitude velocities do occur during winter, but do not frequently exceed 0.30 m s^{-1}. Velocity profiles at Papa are found to exhibit near-inertial oscillations during winter, as is discussed in *Alfords et al. (2012)*.

For ease of display, inverse Richardson numbers (Ri^{-1}) below the mixed layer at KEO and Papa are displayed in **Figure 5**. As a result, $Ri^{-1} > 1$ now indicates potential onset of shear-based turbulence below the mixed layer. At KEO, minima in Ri^{-1} appear to occur during summertime, with values ranging from 1 to 2. In contrast, maxima in Ri^{-1} appear to occur twice a year: once during early spring and once during early fall. During these times, Ri^{-1} frequently exceeds 10, well above established criteria for shear-based turbulence onset.

At Papa, minima in Ri^{-1} also appear to occur during summer months, and the values for these minima range from 0.5 to 1, in almost all cases smaller than values at KEO. Maxima in Ri^{-1} at Papa occur in late spring. During this time, Ri^{-1} ranges from 2 to 4, much smaller than values at KEO and only marginally diagnostic of shear-based turbulence.

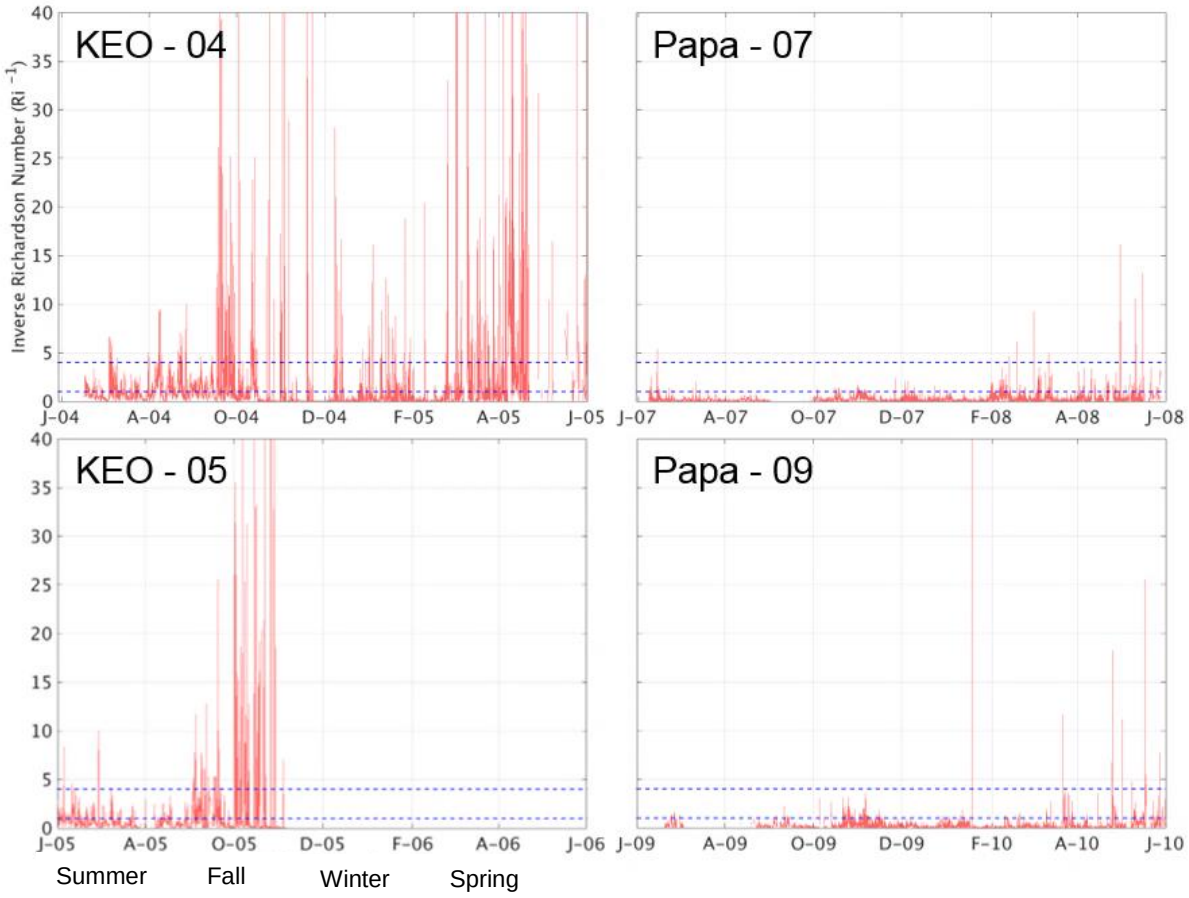

Figure 5. Left panels: hourly inverse Richardson numbers (red) at KEO for June 2004 to 2005 (top) and for June 2005 to 2006 (bottom). Right panels: hourly inverse Richardson numbers (red) at Papa for June 2007 to 2008 (top) and for June 2009 to 2010 (bottom). Richardson numbers ¼ and 1 are plotted in dashed blue lines as reference.

Shear and Stratification Comparisons

Criteria for turbulent onset (Ri < 1 and Ri < ¼) are met or exceeded, and in particular, P_{SBT} at KEO during early spring (March – April) approaches 24 hours day^{-1}, the maximum possible value [**Figure 6**]. Such large values suggest enhanced periods of near-continuous shear instability below the mixed layer in early spring. High values of P_{SBT} are also found during early fall at KEO, averaging ~ 15 hours day^{-1}. In contrast to early spring and fall, P_{SBT} during summer

and early winter at KEO average ~ 6 hours day^{-1}, which corresponds to the smaller Ri^{-1} during this time period.

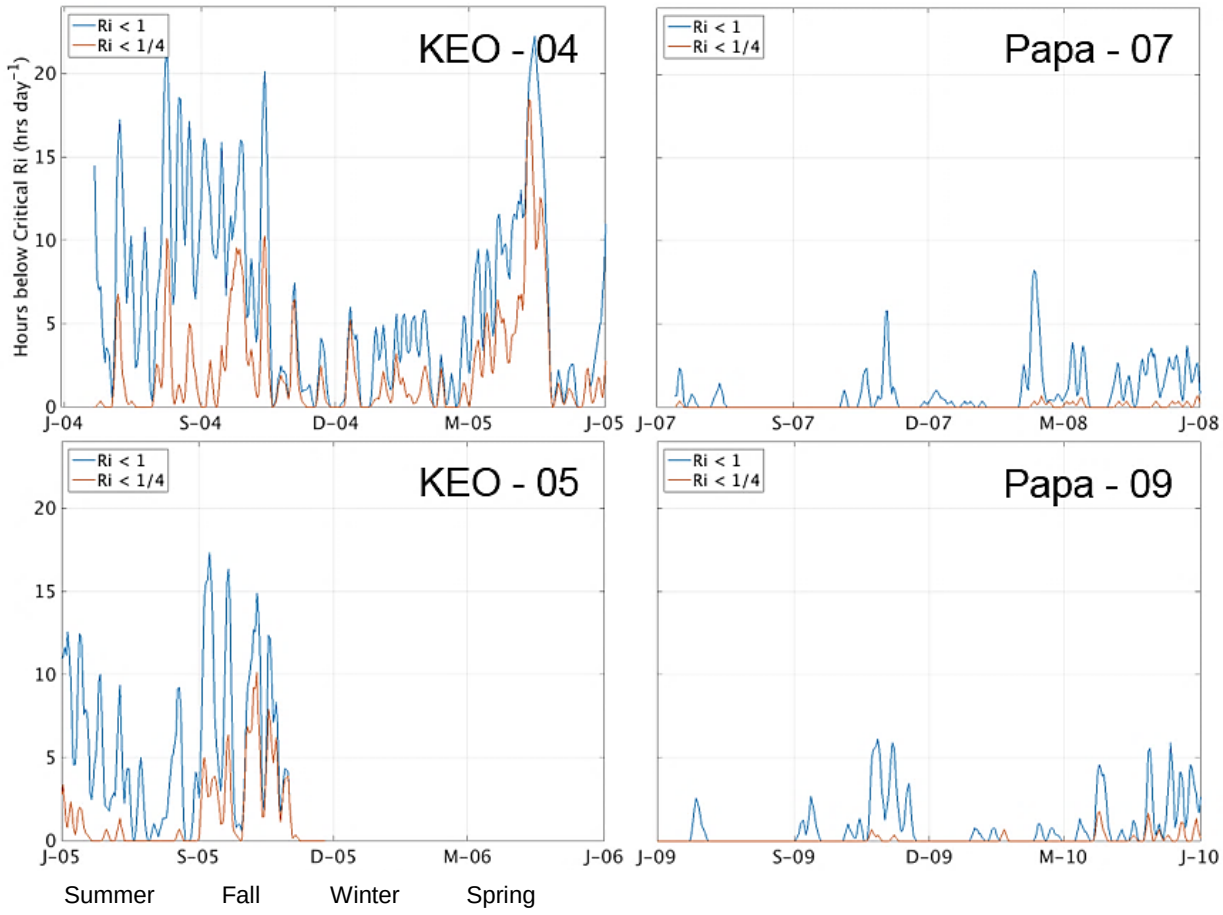

Figure 6. Left panels: 5-day smoothed number of hours per day Richardson number goes critical at KEO during June 2004 to 2005 (top) and during June 2005 and 2006 (bottom). Right panels: 5-day smoothed number of hours per day Richardson number goes critical at Papa during June 2007 to 2008 (top) and during June 2009 to 2010 (bottom). Critical Richardson numbers are taken as 1 (blue) and ¼ (orange).

Large P_{SBT} during early spring at KEO coincides with extremely weak density stratification (~ -5×10^{-3} kg m^{-4}) compared to annual averages, as anticipated. During this period, however, **Figure 7** suggests density stratification when Ri < 1 is stronger than background stratification. Stronger density stratification during turbulent conditions (Ri < 1) appears to be

significantly compensated by enhancement of velocity shears below the mixed layer, which average 4.5 times above shear when Ri > 1.

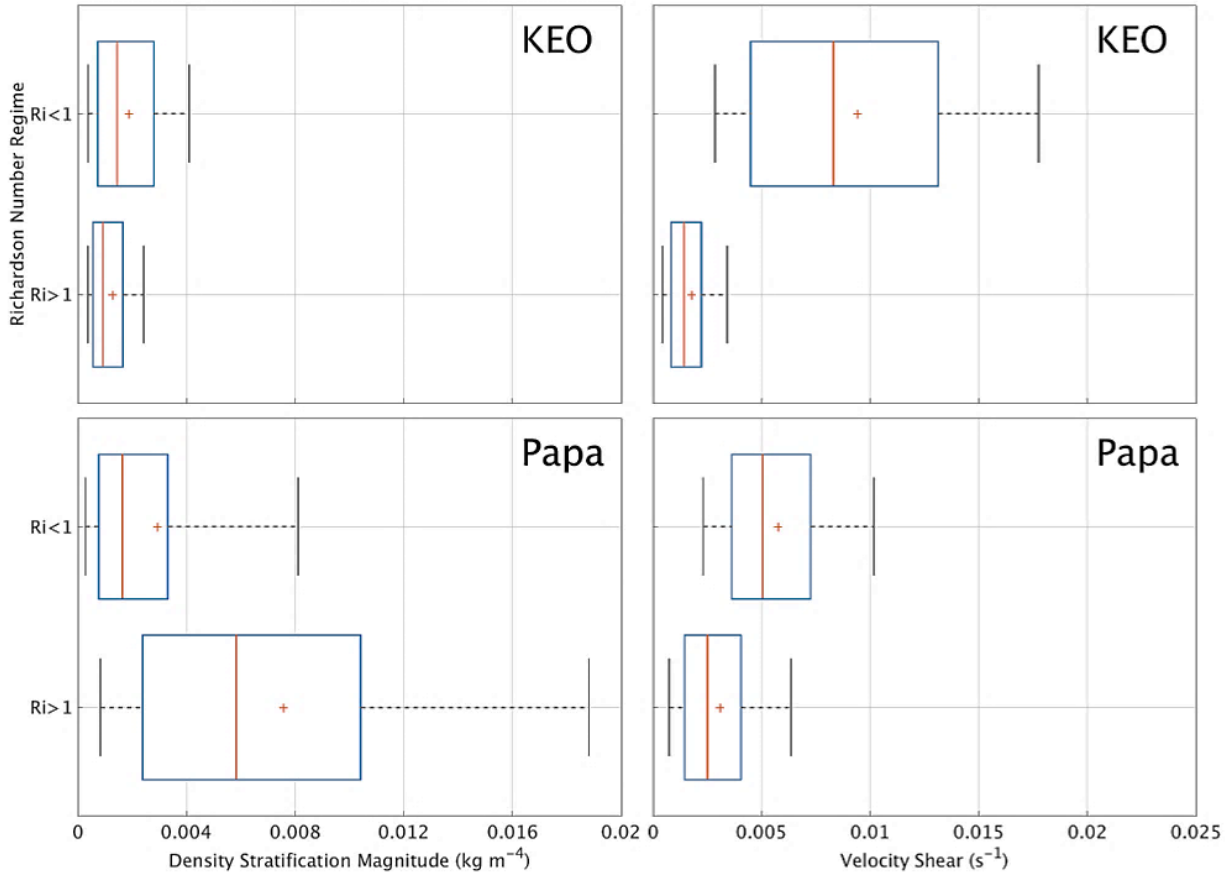

Figure 7. Left panels: absolute value of density stratification at KEO during March-April 2004 (top) and Papa during April-June (bottom) when Ri < 1 and Ri > 1. Right panels: velocity shear at KEO during March-April (top) and Papa during April-June (bottom) when Ri < 1 and Ri > 1. Black lines indicate minima and maxima, blue boxes indicate the interquartile range, and the red lines indicate medians. Red +'s indicate means.

P_{SBT} at Papa is much more sensitive to criteria for onset of shear-based turbulence than at KEO [**Figure 6**]. Such sensitivity is a result of much smaller Ri^{-1} at Papa than at KEO. Nonetheless, during late spring (April to June), average P_{SBT} is ~ 4 hours day^{-1}. A secondary maximum in P_{SBT} appears to occur during late fall, although it fades quickly if the criteria for

shear-based turbulent onset becomes more stringent (closer to ¼). Mid-fall and mid-winter at Papa average near 0 hours day^{-1} of P_{SBT}, emphasizing the rarity of shear instabilities at Papa during other times of the year.

As at KEO, strong prevalence of turbulence during late spring at Papa coincides with extremely weak density stratification (~ -5×10^{-3} kg m^{-3}) compared to annual averages. Moreover, during this period, **Figure 7** suggests median density stratification when Ri < 1 is roughly three times weaker than median stratification when Ri > 1, and median velocity shears when Ri < 1 are roughly twice as strong as median velocity shears when Ri > 1.

Differences in median density stratification (velocity shear) when Ri < 1 and Ri > 1 are found to be statistically different at the 5% significance level between KEO and Papa according to Mood's statistic [**Table 2**]. Indeed, Mood's statistic for density stratification below the mixed layer is larger at Papa than at KEO, suggesting weakening density stratification is more associated with low Ri conditions at Papa. In contrast, Mood's statistic for velocity shear below the mixed layer is much larger at KEO than at Papa, suggesting strengthening velocity shear in the presence of weak stratification is more associated with low Ri conditions at KEO, as seen in **Figure 7**. Such results indicate fundamental differences in set-up of shear-based turbulence below the mixed layer between the two moorings.

Table 2. Results of Mood's test for differences in median density stratification when Ri < 1 and Ri > 1 (first two columns) and differences in median velocity shear when Ri < 1 and Ri > 1 (last two columns) at KEO during March – April and Papa during April – June.

	Stratification	**Velocity Shear**
KEO	43	647
Papa	160	106

Richardson Number and Diffusivity Associations

5-day smoothed daily P_{SBT} and diffusivities are displayed at KEO in the leftmost panels of **Figure 8**. Mean periodicity of peaks in P_{SBT} is T ~ 6.6 ± 0.4 days during summer and fall and is statistically indistinguishable from that of diffusivities at the 5% significance level. Mean distance between peaks in P_{SBT} and peaks in diffusivities is d_f ~ 2.5 ± 0.5 days, and peaks in P_{SBT} precede peaks in diffusivities as often as peaks in diffusivities proceed peaks in P_{SBT}. Therefore, while peaks in P_{SBT} and diffusivities may share similar periods, little evidence of phase relationship between these peaks is found on average.

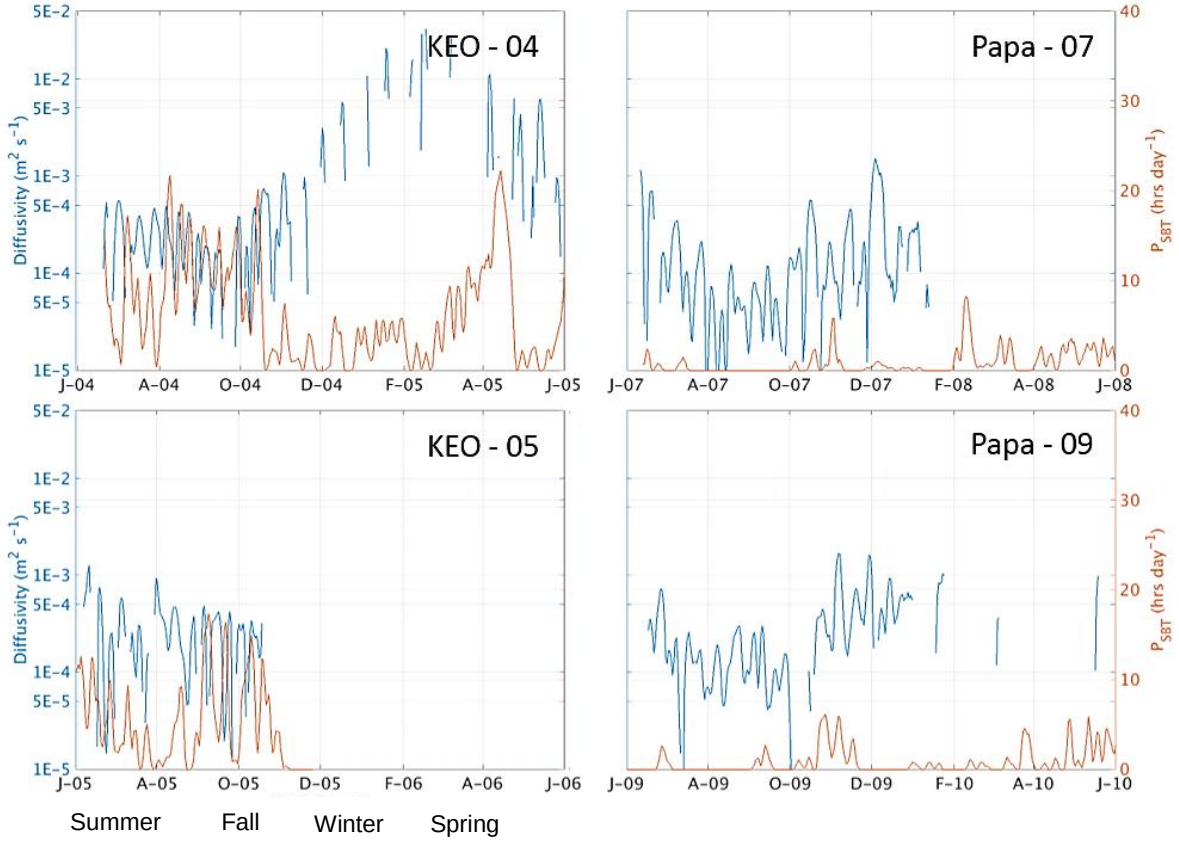

Figure 8. Left panels: 5-day smoothed diffusivity (blue) and P_{SBT} (orange) below the mixed layer at KEO during June 2004 to 2005 (top) and during June 2005 to 2006 (bottom). Right panels: 5-day smoothed diffusivity (blue) and P_{SBT} (orange) below the mixed layer at Papa during June 2007 to 2008 (top) and during June 2009 to 2010 (bottom).

Power spectra of P_{SBT} and 5-day smoothed P_{SBT} are in good agreement beyond periods of ~ 5.8 days at KEO during late summer to early fall (August through September). In addition, both power spectra suggest a strong signal of period ~ 6.5 days [**Figure 9**]. Therefore, one can have confidence the peaks observed in the smoothed P_{SBT} are present in the unsmoothed P_{SBT}, and the ~ 6.5 day average separation between these peaks observed in **Figure 8** is not solely a side-effect of the 5-day smoother. It is assumed the 5-day smoother has a similar effect on diffusivities, so that the ~ 6.5 day average separation between peaks in diffusivities in **Figure 8** is also not solely a side-effect of the 5-day smoother.

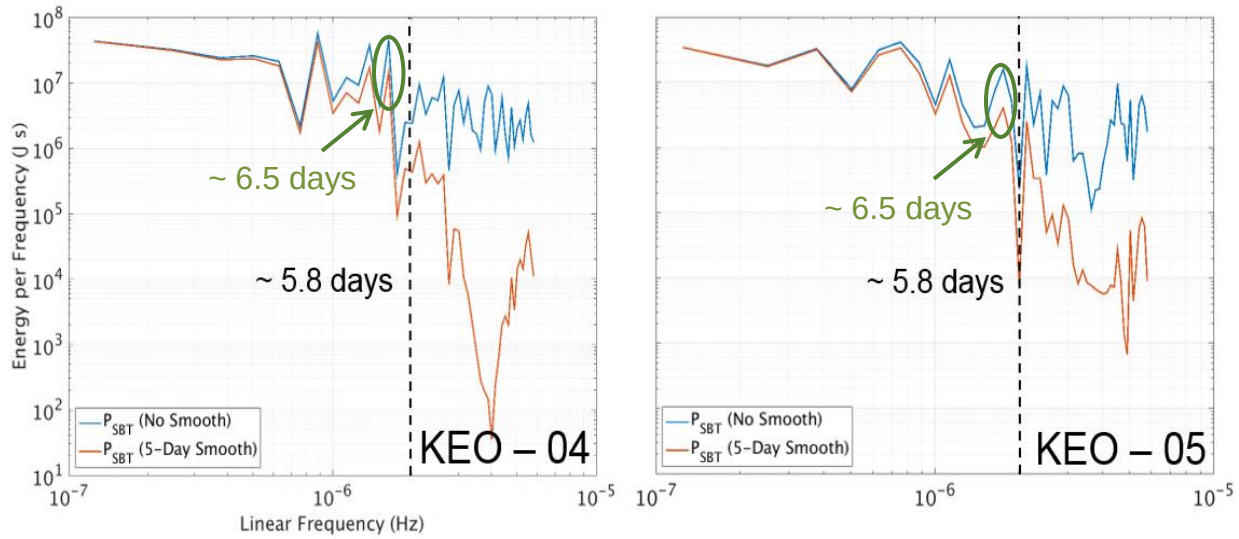

Figure 9. Power spectra (energy per unit frequency) of P_{SBT} (blue) and 5-day smoothed P_{SBT} (orange) at KEO from August to September 2004 (left) and 2005 (right). Frequency at which smoother lessens power by more than 5-fold in black dashed line and ~ 6.5 day periodicity circled in green.

Surface Forcing and Diffusivity Associations

Results of the correlation analysis between diffusivities and surface forcings at KEO and Papa are summarized in **Figure 10** and **Figure 11**, respectively. Standardized regression

coefficients, interpreted as sensitivities to diffusivities to surface forcings, display seasonality in associations between surface forcings and diffusivities at both moorings. These seasonalities appear to be statistically indistinguishable between moorings, as corresponding confidence intervals of regression coefficients display significant overlap.

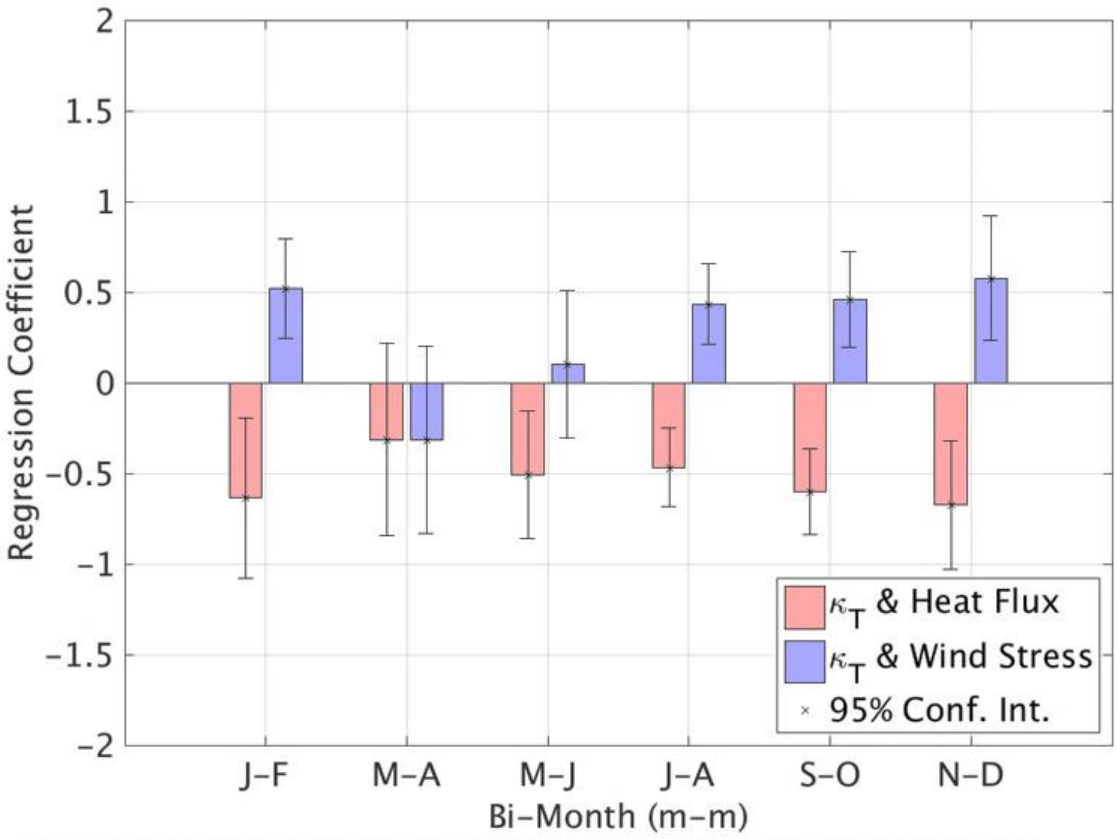

R^2 Statistic	J–F	M–A	M–J	J–A	S–O	N–D
κ_T & Heat Flux	0.41	0.05	0.26	0.22	0.36	0.46
κ_T & Wind Stress	0.27	0.10	0.01	0.19	0.21	0.33

Figure 10. Standardized regression coefficients of 5-day smoothed daily diffusivity against heat flux (red) and against wind stress (blue) per bi-month at KEO. 95% confidence intervals of regression coefficients indicated by error bars. Corresponding R^2 statistic for each regression indicated by chart below.

At KEO, associations between diffusivities and surface forcings are present and indicate statistically significant regression coefficients throughout the year, except during early spring. Correlations between diffusivity and heat flux are negative at all times when regression coefficients are statistically significant. In contrast, correlations between diffusivity and wind stress tend to be positive at all times when regression coefficients are statistically significant.

Magnitudes of regression coefficients are statistically indistinguishable at the 5% significance level between heat flux and wind stress, which suggests diffusivities below the mixed layer are equally sensitive to either surface forcing. Similarity of regression coefficient magnitudes between heat flux and wind stress is also supported by similar values for R^2 statistics, as shown in **Figure 10**. According to these R^2 statistics, heat flux and wind stress account for ~ 20 – 25% of the variance observed in diffusivities below the mixed layer on average, with highest values found during late fall and early winter at KEO alongside strongly significant regression coefficients.

At Papa, associations are statistically strong from January to April [**Figure 11**]. These associations are not statistically different than at KEO at the 5% level. Correlations retain the same signs as at KEO whenever significant: correlations between diffusivities and heat fluxes are negative, while correlations between diffusivities and wind stresses are positive. Magnitudes of regression coefficients during mid-winter to early spring at Papa are statistically indistinguishable between heat flux and wind stress. These similarities are likewise supported by similar R^2 statistics for correlations of diffusivity with surface heat flux and wind stress, as seen in **Figure 11**. Heat flux and wind stress account for ~ 15-40% of variance observed in diffusivities below mixed layer at Papa during mid-winter to early spring. For the rest of the year at Papa, especially during summer months, much weaker associations are observed in regression

coefficients and R^2 statistics between diffusivities below the mixed layer and surface forcings compared to value during mid-winter to early spring.

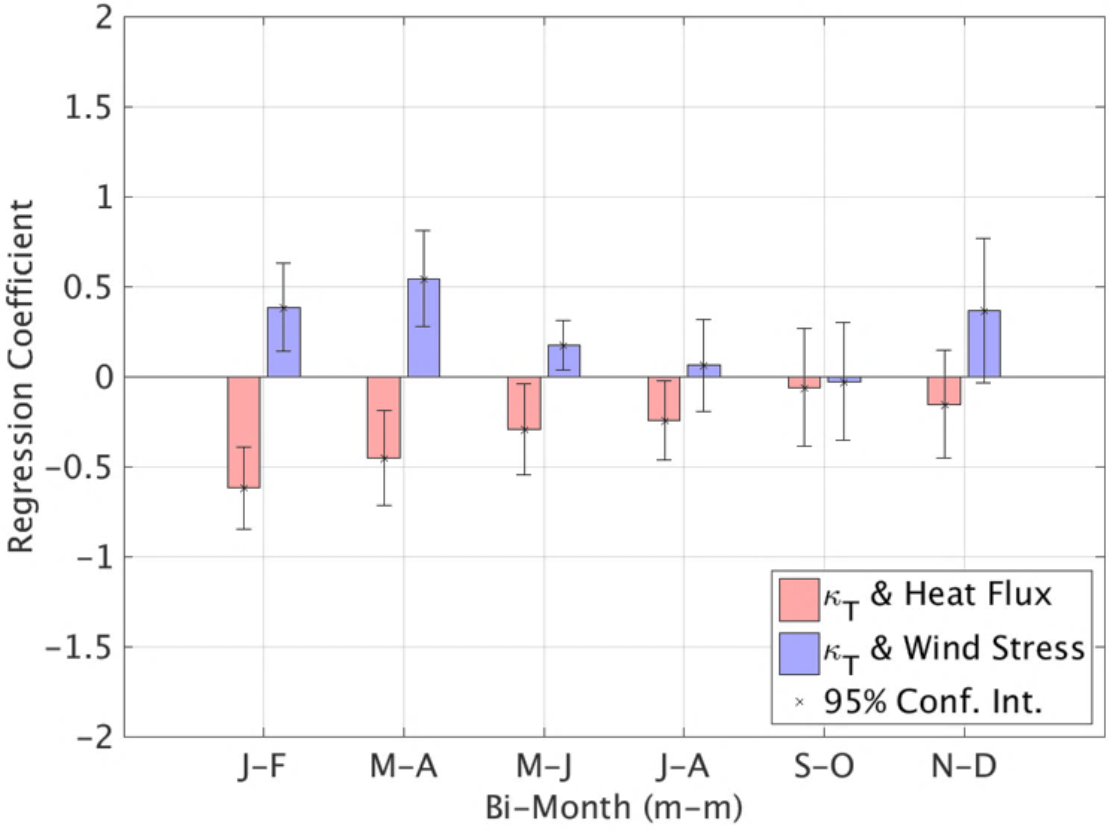

R^2 Statistic						
	0.39	0.21	0.09	0.06	< 0.01	0.02
	0.15	0.30	0.03	< 0.01	< 0.01	0.20

Figure 11. Standardized regression coefficients of 5-day smoothed daily diffusivity against heat flux (red) and against wind stress (blue) per bi-month at Papa. 95% confidence intervals of regression coefficients indicated by error bars. Corresponding R^2 statistic for each regression indicated by chart below.

For bi-months with strong association (statistically significant regression coefficients and high R^2 statistics) at both KEO and Papa, signs are consistent with physical intuition. Given heat loss at the ocean's surface (negative heat flux), surface water parcels will sink below the mixed

layer, enhancing turbulent mixing [*Large et al.,1986, Large et al., 1994*]. Moreover, given stronger wind stress at the ocean's surface, momentum will be transferred throughout the mixed layer, eventually stirring up turbulence below mixed layer base [*Skyllingstad et al., 2000*].

Chapter 6

Discussion

Overview of Results

Richardson numbers provide a constraint on the onset of shear-based turbulence initiated by weak density stratification and strong velocity shear. In this analysis, Richardson numbers below the mixed layer are smallest during early spring (March-April) at KEO and mid-to-late spring (April-June) at Papa. Moreover, Richardson numbers at KEO are almost always smaller than at Papa, sometimes by an order of magnitude during spring and fall [**Figure 4**].

Peaks in prevalence of shear-based turbulence (P_{SBT}), defined as the number of hours per day when Ri < 1 below the mixed layer, are found to be spaced ~ 6.5 days apart at KEO from late summer to fall, which matches that in diffusivities below the mixed layer for both moorings. Thus, shear-based turbulence and general turbulent diffusion share similar modes of weekly variability during certain times of the year at KEO.

Surface heat flux and wind stress are strongly associated with diffusivities below the mixed layer at all times throughout the year at KEO outside early spring (March – April), while surface forcings are only associated with diffusivities during winter months (November – February) at Papa. Thus, differences in local meteorology may provide additional insight into behavior of turbulent diffusion below the mixed layer at KEO and Papa, particularly during late fall and early winter.

OCS KEO

Small Richardson numbers at KEO during spring coincide with weak stratification below the mixed layer, which is found to be an order of magnitude smaller than the annual mean stratification of ~ -0.03 kg m^{-4}. During this period, stratifications corresponding to Ri < 1 become slightly stronger than those for Ri > 1, and not weaker as expected [**Figure 6**]. Instead, velocity shears are found to be significantly larger for Ri < 1, which suggests weak stratification alone is not responsible for instabilities below mixed layer base. Rather, while weak stratification provides greater predisposition to turbulent onset, sufficiently strong velocity shears are paramount to initiating turbulence below mixed layer at KEO during early spring.

Springtime P_{SBT} at KEO appears to occur just prior to the reformation of the seasonal pycnocline. Indeed, in **Figure 3**, buoyancy frequencies wane in late March and begin to rebound through mid-April. *Hosegood et al. (2008)* and *Cronin et al. (2013)* find strong horizontal advective processes to be a precursor to seasonal pycnocline development. These advective processes may be responsible for the enhanced velocity shears observed during early spring at KEO and help to account for the strong dependence of shear-based turbulence onset on velocity shears found during this time period.

A complementary explanation for high P_{SBT} during this period may be the result of a ventilating layer of near isothermal water situated between mixed layer base and the permanent pycnocline known as subtropical mode water (STMW). STMW near KEO develops as a result of strong surface buoyancy loss from the preceding winter, reaches peak vertical extent around March and April, and gradually erodes with the redevelopment of the seasonal pycnocline [*Qiu et al., 2007*]. As a result, the presence of near isothermal water below the mixed layer may

account for the extremely weak density stratification observed at KEO during March and April and, thus, precondition KEO's mixed layer base for shear-based turbulence.

Strong extratropical cyclones during early spring at KEO may also present possibilities for wind-generated NIOs to instigate velocity shears below the mixed layer strong enough to instigate shear-based turbulence, though it is suspected that the mixed layer base may be too far removed from the surface during this time period. Indeed, velocity shears in **Figure 3** seem to support such a disconnect between the surface and the mixed layer base, as one would expect velocity shears to increase during winter from the presence of strong NIOs, not decrease. Moreover, power spectra of velocities below mixed layer at KEO (not shown) only show slight enhancement of energy at the inertial frequency, which suggests other processes are equally responsible for velocity and its shear below the mixed layer at KEO.

It is more likely that NIOs are responsible for high prevalence of shear-based turbulence below the mixed layer in early fall (September to October) at KEO, when strong tropical cyclones occur frequently [*Bond et al., 2011*]. Indeed, Category 4 + cyclones that pass nearby KEO during this investigation include Meari (09/20/04 – 09/29/04), Ma-On (09/29/04 – 10/10/2004), and Kirogi (10/10/05 – 10/19/05) [*Tomita et al., 2010*]. From **Figure 5**, it appears Richardson numbers go critical for a few days during each of these events, as anticipated: with KEO's mixed layer depth remaining steady and shallow at ~ 15 to 20 m, previous studies of bulk mixed layer models have indicated considerable wind stress influence at and below mixed layer depth up to several tens of meters deep [*D'Asaro, 1985a*; *Crawford & Large, 1996; Plueddemann & Farrar, 2006*].

Local peaks in prevalence of shear-based turbulence and diffusivities during fall also display similar periodicity (T ~ 6.5 days) at KEO. Perhaps the frequency of these peaks is

associated with the frequency of passing weather systems—both tropical and extra-tropical. A future case study of fall 2004 at KEO, in particular, may help to clarify this connection, as peaks in prevalence of shear-based turbulence and diffusivities are found to be well co-located throughout August, September, and October of this year.

In addition to influence of wind stress on shear-based turbulence and diffusivities below the mixed layer, a recent investigation in the North Atlantic Ocean suggests wind-generated NIOs in the presence of the Gulf Stream front initiate symmetrically unstable flows in the upper ocean that can temporarily weaken stratification and enhance shear-based turbulence [*Thomas et al., 2016*]. KEO's close proximity to the Kuroshio front may, therefore, provide an alternative explanation for high prevalence of shear-based turbulence below the mixed layer during fall.

OCS Papa

At Papa, shear-based turbulence below the mixed layer is most prevalent during mid-to-late spring as opposed to early spring at KEO. This slight difference in timing of maximum P_{SBT} between the two moorings appears to be driven by differences in the seasonality of buoyancy frequencies. In particular, while buoyancy frequency at KEO begins to increase during mid-April, buoyancy frequency at Papa continues to decrease through May, beginning its increase in early June. Despite these differences, strong prevalence of shear-based turbulence below the mixed layer immediately precedes the development of the seasonal pycnocline at Papa, just as at KEO.

Unlike at KEO, shear-based turbulence at Papa relies on further weakening of density stratification below the mixed layer, as seen in **Figure 7**. Moreover, Mood's statistics for density stratification and velocity shears below the mixed layer when Ri < 1 and Ri > 1 are much closer at Papa than those at KEO, which suggests density stratification and velocity shear contribute fairly equally to onset of shear-based turbulence at Papa [**Table 2**].

Density stratification and velocity shear necessary for onset of shear-based turbulence during late spring may be influenced by surface buoyancy loss and wind stress from passing extratropical systems. Indeed, correlations between surface heat flux, wind stress, and diffusivities are most robust during late spring, which may indirectly suggest surface forcings have some bearing on density stratification and velocity shear below the mixed layer during this period [**Figure 10**]. Previous investigations have also suggested associations among conditions below the mixed layer, surface wind stress [*D'Asaro, 1985b*], and solar insolation [*Large et al., 1986*] at the ocean's surface.

In comparison to late spring, all other seasons at Papa experience considerably less frequent shear-based turbulence below the mixed layer, especially if one considers critical Richardson numbers < ¼ as a criteria for onset of shear-based turbulence. Given this weak signal in combination with large data gaps in diffusivities, little connections can be drawn between peaks in prevalence of shear-based turbulence and peaks in diffusivities at Papa at this time. Such a conclusion may illustrate a limitation of the data available in this investigation or suggest shear-based turbulence is not frequently a primary mechanism for turbulent diffusion below the mixed layer at Papa.

Despite the lack of convincing evidence for connections between prevalence of shear-based turbulence and diffusivities at Papa, **Figure 5** suggests some evidence for a secondary

maximum in shear-based turbulence from November to December. Similar to KEO, this secondary maximum may be associated with NIOs from passing extratropical systems, as correlations between diffusivities and wind stress are found to be strong and positive during this time. Analysis of Storm Transfer and Response Experiment data at Papa for a 14-day period in November 1980 suggests Richardson numbers below mixed layer are found to increase as a result of enhanced variability in near-inertial shear preceding passages of cold fronts [*D'Asaro, 1985b*]. Estimates of these Richardson numbers were found to be ~ 2.5 in the background flow and ~ 0.7 in shear-based turbulent conditions, consistent with Richardson numbers found in this study during the same time of year [**Figure 5**].

Regressions of diffusivities against surface heat flux and wind stress at Papa during late fall and winter (November to February) suggest local meteorological forcings could be of first-order importance for turbulent diffusion below the mixed layer, especially given that R^2 statistics suggest these surface forcings account for ~ 25% of the variance observed in diffusivities on average. In contrast, weak regressions of diffusivities against surface heat flux and wind stress at Papa during summer months (June, July, August) suggest local meteorological forcings are not likely to be of first-order importance for turbulent diffusion below the mixed layer during this time. Given shear-based turbulence is also weak during this period, there must be another process responsible for turbulent diffusion during summer at Papa. Such processes might include double-diffusion, salt fingering, Langmuir turbulence, or internal solitary waves generated by tidal forcings.

Surface Forcing and Diffusivity Associations

Parameterizations of upper-ocean diffusivities are necessary to model the fluxes of heat, momentum, and freshwater between the ocean's surface and its interior. These parameterizations typically derive from sophisticated closure schemes or similarity arguments, often at the expense of physical interpretability. Herein, associations are drawn directly between diffusivities and surface forcings such as heat flux and wind stress for purposes of physical interpretability and not mathematical sophistication. Nonetheless, signs of heat flux and diffusivity associations in this study are found not only to be interpretable, but are also consistent with predictions from a simple diffusivity and mixed layer model parameterization.

Results from this study suggest negative associations between surface heat flux and diffusivities at both KEO and Papa. Physical interpretation of these negative associations may imply negative surface heat fluxes induce surface buoyancy loss, which then enhances turbulent diffusion through convective overturning cells that penetrate the base of the mixed layer according to *Large et al. (1986)* and *Large et al. (1994).*

From the work of *Osborn (1980)* and *Gargett & Holloway (1984),* a simple parameterization of diffusivity κ_T may be constructed as follows:

$$[Eqn. 8] \qquad \kappa_T = \Gamma \frac{\varepsilon}{N^2}$$

where Γ is a non-dimensional mixing efficiency (a function of flux Richardson number) and ε is eddy kinetic energy dissipation resulting from viscous stresses acting on deforming fluid parcels. ε may be estimated from fine- and microstructure measurements of velocity shear at the centimeter scale and molecular viscosity of seawater [*Ledwell et al., 2011*]. However, ε is

typically parameterized as a decreasing function of *N* based on the conceptual notion that stronger fluid stratification should mitigate effects of dissipation on turbulent eddies. Assuming ε does vary inversely with *N* and assuming constant mixing efficiency, one finds diffusivity below mixed layer may be expressed as a decreasing function of *N*. Assuming *N* below mixed layer is controlled by some fraction of surface heat flux, as is frequently done in vertically integrated mixed layer models and Bowen-ratio methods in the atmosphere [*Stull, 1988*], one finds diffusivity below the mixed layer is necessarily a decreasing function of surface heat flux. Indeed, diffusivity and surface heat flux were consistently negatively correlated in this investigation.

Connections between [*Eqn. 8*] and the positive associations found in this analysis between diffusivities below the mixed layer and wind stress are not as readily observed. It may be that wind stress contributes strongly to local velocity shears below the mixed layer as considered in *Skyllingstad et al. (2000)*. If such is the case, a working hypothesis is to consider relationships between surface wind stress and Γ, ε, and/or N below the mixed layer.

Future Work

Pertinent to understanding seasonal and regional variability of turbulent diffusion below the mixed layer is an understanding of the sources for this mixing. In this analysis, relationships between diffusivity and a metric for shear-based turbulence: the number of hours per day for which Ri < 1, or P_{SBT}. Correlation analysis between diffusivities and surface fluxes of heat and momentum have also been performed. There are several other processes, however, which may

affect diffusivity below the mixed layer, chief among which are surface gravity waves and associated Langmuir turbulence [*Polton et al., 2008; D'Asaro 2014*].

Indeed, provided ADCP velocities are made available for longer time periods in the future, one can begin to establish associations between diffusivities and Langmuir turbulence, or other surface-driven processes, in much the same way as has been done herein with shear-based turbulence below the mixed layer. Through these surface forcings, one might build stronger connections between upper and lower boundaries of the ocean's mixed layer, understand how these connections transpire across multiple time scales, and further bridge the gap between Richardson numbers calculated in this thesis and diffusivities calculated in *Cronin et al. (2015).* In addition, given higher resolution ADCP velocities and diffusivity measurements, one may be able to better infer the quality of diffusivity parameterizations (or lack thereof) in upper-ocean turbulence models below the mixed layer.

With even longer hourly ADCP measurements (> 10 years), one can begin to discuss not only seasonal and regional variability of shear-based turbulence below mixed layer, but also inter-annual variability of this turbulence. The effect of inter-annual variability in shear-based turbulence on turbulent diffusion below the mixed layer may then be studied as well as its effects on marine biogeochemistry.

Thus, this thesis takes an incremental step towards the much larger goal of understanding how turbulent diffusion below the mixed layer varies at different time scales and locations in the world's oceans and how such variability may have implications on the physical, chemical, and biological state of the oceans.

Chapter 7

Conclusion

The scientific motivation for this investigation developed from seasonal and regional variability discovered in diffusivities below the mixed layer at two NOAA North Pacific moorings KEO and Papa. In particular, *Cronin et al. (2015)* found monthly and 5-day averaged diffusivities peaked during March and April at both moorings, and diffusivities at KEO were larger than at Papa year-round. In this study, seasonal and regional variability of shear-based turbulence, a subset of processes potentially responsible for turbulent diffusion below mixed layer, was investigated. Associations between diffusivities below the mixed layer and surface forcings such as surface heat flux and wind stress were also determined for various bi-months throughout the year at KEO and Papa.

Prevalence of shear-based turbulence, defined as the number of hours per day when $Ri < 1$, was found to be largest during March to April at KEO and April to June at Papa, just prior to the development of the season pycnocline. Moreover, shear-based turbulence occurred much more frequently at KEO than at Papa year-round. Peaks in prevalence of shear-based turbulence at KEO were found to exhibit periodicity of ~ 6.5 days from late summer to fall, matching that in diffusivities—despite smoothing effects. Consequently, shear-based turbulence exhibited some similar modes of variability to diffusivities associated with turbulent diffusion below the mixed layer at KEO. This connection was muted at Papa due to lack of continuous diffusivity measurements. Therefore, this work implies shear-based turbulence, while consistent with some features of seasonal and regional variability in diffusivities, is still an ongoing investigation.

Surface heat flux and wind stress were found to correlate strongly and equally with diffusivities below the mixed layer throughout different times of the year at both KEO and Papa. These associations demonstrated seasonality, and these seasonalities were found to be similar between the two moorings in the sense that corresponding regression coefficients were not statistically different between moorings. Diffusivities correlated significantly with surface forcings outside March to April at KEO, while diffusivities correlated significantly with surface forcings during late fall and winter at Papa. Significant associations during late fall and winter at both moorings were found to account for ~ 25 % of observed variability in turbulent diffusion below the mixed layer on average.

In future work, one can begin to investigate not only seasonal and regional variability of turbulent diffusion, but also its inter-annual variability and connections with other surface processes, such as waves and Langmuir turbulence. In so doing, future work may characterize turbulent diffusion below the mixed layer on multiple time scales and better connect shear-based turbulence discussed herein, diffusivities derived in *Cronin et al. (2015)*, and popular diffusivity parameterizations implicitly involving surface forcings. Thus, this thesis provides the first step in understanding how turbulent diffusion varies on seasonal and regional scales, allowing future work to determine this variation on other scales as well as consider its implications on physical, chemical, and biological variables dependent on this mixing process.

BIBLIOGRAPHY

Abarbanel, H. D. I., D. D. Holm, J. E. Marsden, and T. Ratiu (1984), Richardson number criteria for the nonlinear stability of a three-dimensional stratified flow, *Physical Review Letters, 52,* 2352 – 2355, doi: http://dx.doi.org/10.1103/PhysRevLett.52.2352.

Alford, M. H., M. F. Cronin, and J. M. Klymak (2012), Annual cycle and depth penetration of wind-generated near-inertial waves at Ocean Station Papa in the northeast Pacific, *J. Phys. Oceanogr., 42(6),* 889 – 909, doi: http://dx.doi.org/10.1175/JPO-D-11-092.1.

Andrews, D. W. K. (1991), Heteroskedasticity and autocorrelation consistent covariance matrix estimation, *Econometrica, 59,* 817 – 858, doi: 10.2307/293822.

Bendat, J. S. and A. G. Piersol (2011), Random Data: Analysis and Measurement Procedures, Third Edition, *John Wiley & Sons,* pp. 640.

Bond, N. A., M. F. Cronin, C. Sabine, Y. Kawai, H. Ichikawa, P. Freitag, and K. Ronnholm (2011), Upper-ocean response to typhoon Choi-Wan as measured by the Kuroshio Extension Observatory (KEO) mooring, *J. Geophys. Res., 116,* C02031, doi: 10.1029/2010JC006548.

Breusch, T. S. and A. R. Pagan (1979), A simple test for heteroscedasticity and random coefficient variation, *Econometrica, 47,* 1287 – 1294, doi: 10.2307/1911963.

Brown, G. M. and A. M. Mood (1951), On median tests for linear hypotheses, *Proceedings of the Second Berkeley Symposium on Mathematical Statistics and Probability, University of California Press, Berkeley, Calif.,* 159 – 166.

Canuto, V. M., A. Howard, Y. Cheng, and M. S. Dubovikov (2001): Ocean turbulence, part I: One-point closure model—momentum and heat vertical diffusivities, *J. Phys. Oceanogr.*, *31*, 1413 – 1426.

Cronin, M. F., N. A. Bond, J. T. Farrar, H. Ichikawa, S. R. Jayne, Y. Kawai, M. Konda, B. Qiu, L. Rainville, and H. Tomita (2013), Formation and erosion of the seasonal thermocline in the Kuroshio Extension recirculation gyre, *Deep-Sea Res., Part II, 85*, 62 – 74, doi: 10.1016/j.dsr2.2012.07.018.

Cronin, M. F., N. A. Pelland, S. R. Emerson, and W. R. Crawford (2015), Estimating diffusivity from heat and salt balances in the north Pacific, *J. Geophys. Res.-Oceans, 120*, 7346 – 7362, doi: 10.1002/2015JC011010.

D'Asaro, E. A. (1985a), The energy flux from wind to near-inertial motions in the surface layer, *J. Phys. Oceanogr., 15*, 1043 – 1059, doi: http://dx.doi.org/10.1175/1520-0485(1985)015<1043:TEFFTW>2.0.CO;2.

D'Asaro, E. A. (1985b), Upper ocean temperature structure, inertial currents, and Richardson numbers observed during strong meteorological forcing, *J. Phys. Oceanogr., 15*, 943 – 962. doi: http://dx.doi.org/10.1175/1520-0485(1985)015<0943:UOTSIC>2.0.CO;2.

D'Asaro, E. A. (2014), Turbulence in the upper-ocean mixed layer, *Annual Review of Marine Science, 6*, 101 – 115, doi: 10.1146/annurev-marine-010213-135138.

de Boyer Montégut, C., G. Madec, A. S. Fischer, A. Lazar, and D. Iudicone (2004), Mixed layer depth over the global ocean: An examination of profile data and a profile-based climatology, *J. Geophys. Res., 109*, C12003, doi: 10.1029/2004JC002378.

Fairall, C.W., E. F. Bradley, J. E. Hare, A. A. Grachev, and J. B. Edson (2003), Bulk parameterization of air-sea fluxes: updates and verification for the COARE algorithm,

J. Climate, 16, 571 – 591, doi: http://dx.doi.org/10.1175/1520-0442(2003)016<0571:BPOASF>2.0.CO;2.

Fassbender, A. J., C. L. Sabine, and M. F. Cronin (2016), Net community production and calcification from seven years of NOAA Station Papa Mooring measurements, *Global Biogeochem. Cycles, 30*, doi: 10.1002/2015GB005205.

Freitag, H. P., M. McCarty, C. Nosse, R. Lukas, M. J. McPhaden, and M. F. Cronin (1999), COARE SEACAT data: Calibration and quality control procedures, NOAA Tech. Memo. *ERL PMEL, 115*, pp. 89.

Galperin, B., S. Sukoriansky, and P. S. Anderson (2007), On the Richardson number in stably stratified turbulence, *Atmospheric Science Letters, 8*, 65 – 69, doi: 10.1002/asl.153.

Gargett, A. E. and G. Holloway (1984), Dissipation and diffusion by internal wave breaking, *Journal of Marine Research, 42*, 15 – 27, doi: http://dx.doi.org/10.1357/002224084788506158.

Garrett, C. and W. Munk (1979), Internal waves in the ocean, *Annual Review of Fluid Mechanics, 11*, 339 – 369.

Griffies, S. M., M. Winton, W. G. Anderson, R. Benson, T. L. Delworth, C. O. Dufour, J. P. Dunne, P. Goddard, A. K. Morrison, A. Rosati, A. T. Wittenberg, J. Yin, and R. Zhang (2015), Impacts on ocean heat from transient mesoscale eddies in a hierarchy of climate models, *J. Climate, 28*, 952 – 977, doi: http://dx.doi.org/10.1175/JCLI-D-14-00353.1.

Holton, J. R. and G. J. Hakim (2013), An Introduction to Dynamic Meteorology, Fifth Edition, *Elsevier*, pp. 532.

Hosegood, P. J., M. C. Gregg, and M. H. Alford (2008), Restratification of the surface mixed layer with submesoscale lateral density gradients: Diagnosing the importance of the horizontal dimension, *J. Phys. Oceanogr., 38*, 2438 – 2460, doi: http://dx.doi.org/10.1175/2008JPO3843.1.

Howard, L. N. (1961), Note on a paper of John W. Miles, *Journal of Fluid Mechanics, 10*, 509 – 512, doi: http://dx.doi.org/10.1017/S0022112061000317.

Johnson, J. W. and J. M. LeBreton (2004), History and use of relative importance indices in organizational research, *Organizational Res. Methods, 7*, 238 – 257, doi: 10.1177/1094428104266510.

Large, W. G. and G. B. Crawford (1996), Observations and simulations of upper-ocean response to wind events during the Ocean Storms Experiment, *J. Phys. Oceanogr., 25*, 2831-2852.

Large, W. G., J. C. McWilliams, and P. P. Niller (1986), Upper ocean thermal response to autumnal forcing of the northeast Pacific, *J. Phys. Oceanogr., 16*, 1524 – 1550, doi: http://dx.doi.org/10.1175/1520-0485(1986)016<1524:UOTRTS>2.0.CO;2.

Large, W. G., J. C. McWilliams, and S. C. Doney (1994), Oceanic vertical mixing: A review and a model with a nonlocal boundary layer parameterization, *Rev. Geophys., 32*, 363 – 403.

Ledwell, J. R., L. C. St. Laurent, J. B. Girton, and J. M. Toole (2011), Diapycnal mixing in the Antarctic circumpolar current, *J. Phys. Oceanogr., 41*, 241 – 246, doi: http://dx.doi.org/10.1175/2010JPO4557.1.

Mahadevan, A., E. D'Asaro, C. Lee, M. J. Perry (2012), Eddy-driven stratification initiates north Atlantic spring phytoplankton blooms, *Science*, *337*, 54 – 58, doi: 10.1126/science.1218740.

McAuliffe, R. E. (2005), Durbin-Watson statistic, *Wiley Encyclopedia of Management*, *8*, doi: 10.1002/9781118785317.weom080142.

Miles, J. W. (1961), On the stability of heterogeneous shear flows, *Journal of Fluid Mechanics, 10*, 496 – 508, doi: http://dx.doi.org/10.1017/S0022112061000305.

Millero, F. J. and A. Poisson (1981), International one-atmosphere equation of state of seawater, *Deep-Sea Res., Part A. Oceanographic Research Papers*, *28*, 625 – 629, doi: 10.1016/0198-0149(81)90122-9.

Mizuno, K and W. B. White (1983), Annual and interannual variability in the Kuroshio current system, *J. Phys. Oceanogr., 13*, 1847 – 1867, doi: http://dx.doi.org/10.1175/1520-0485(1983)013<1847:AAIVIT>2.0.CO;2.

Montgomery, D. C. and G. C. Runger (2011), Applied Statistics and Probability for Engineers, Fifth Edition, *John Wiley & Sons*, pp. 764.

Nihoul, J. C. J. and Jamart, B. M. (1988), Small-scale Turbulence and Mixing in the Ocean, *Elsevier Science Publishers*, pp. 541.

Osborn, T. R. (1980), Estimates of the local rate of diffusion from dissipation measurements, *J. Phys. Oceanogr., 10*, 83 – 89, doi: http://dx.doi.org/10.1175/1520-0485(1980)010<0083:EOTLRO>2.0.CO;2.

Paternoster, R., R. Brame, P. Mazerolle, and A. Piquero (1998), Using the correct statistical test for the equality of regression coefficients, *Criminology, 36*, 859 – 866, doi: 10.1111/j.1745-9125.1998.tb01268.x.

Plueddemann, A. J. and J. T. Farrar (2006), Observations and models of the energy flux from the wind to mixed-layer currents, *Deep-Sea Res., Part II, 53*, 5 – 30, doi: 10.1016/j.dsr2.2005.10.017.

Polton, J. A., J. A. Smith, J. A. MacKinnon, and A. E. Tejada-Martínez (2008), Rapid generation of high-frequency internal waves beneath wind and wave forced oceanic surface mixed layer, *Geophysical Research Letters, 35*, doi: 10.1029/2008GL033856.

Qiu, B. and A. Kelly (1993), Upper-ocean heat balance in the Kuroshio Extension region, *J. Phys. Oceanogr., 23*, 2027 – 2041, doi: http://dx.doi.org/10.1175/1520-0485(1993)023<2027:UOHBIT>2.0.CO;2.

Qiu, B. and S. Chen (2005), Variability of the Kuroshio Extension jet, recirculation gyre, and mesoscale eddies on decadal time scales, *J. Phys. Oceanogr., 35*, 2090 – 2103, doi: http://dx.doi.org/10.1175/JPO2807.1.

Qiu, B., S. Chen, and P. Hacker (2007), Effect of mesoscale eddies on subtropical mode water variability from the Kuroshio Extension System Study (KESS), *J. Phys. Oceanogr., 37*, 982 – 1000, doi: http://dx.doi.org/10.1175/JPO3097.1.

Skyllingstad, E. D., W. D. Smyth, and G. B. Crawford (2000), Resonant wind-driven mixing in the ocean boundary layer, *J. Phys. Oceangr., 30*, 1866 – 1890, doi: http://dx.doi.org/10.1175/1520-0485(2000)030<1866:RWDMIT>2.0.CO;2.

Shay, L. K., P. G. Black, A. J. Mariano, J. D. Hawkins, and R. L. Elseberry (1992), Upper ocean response to Hurricane Gilbert, *J. Geophys. Res., 97*, 20,227 – 20,248.

Stevenson, J. W. and P. P. Niiler (1983), Upper ocean heat budget during the Hawaii-to-Tahiti shuttle experiment, *J. Phys. Oceanogr., 13*, 1894 – 1907, doi: 10.1175/1520-0485(1983)013<1894:UOHBDT>2.0.CO;2.

Stull, R. B. (1988), An Introduction to Boundary Layer Meteorology, *Springer*, pp. 670.

Tomita, H., S. Kako, M. F. Cronin, and M. Kubota (2010), Preconditioning of the wintertime mixed layer at the Kuroshio Extension Observatory, *J. Geophys. Res.-Oceans, 115*, C12053, doi: 10.1029/2010JC006373.

Thomas, L. N., J. R. Taylor, E. A. D'Asaro, C. M. Lee, J. M. Klymak, and A. Shcherbina (2016), Symmetric instability, inertial oscillations, and turbulence at the Gulf Stream front, *J. Phys. Oceanogr., 46*, 197-217, doi: http://dx.doi.org/10.1175/JPO-D-15-0008.1.

van Haren, H. and L. Gostiaux (2012), Detailed internal wave mixing above a deep-ocean slope, *Journal of Marine Research, 70*, 173 – 197, doi: http://dx.doi.org/10.1357/002224012800502363.

Woods, J. D. (1968), Wave-induced shear instability in the summer thermocline, *Journal of Fluid Mechanics, 32*, 791 – 800. doi:10.1017/S0022112068001035.